Local Measurement of the Superfluid Density in the Pnictide Superconductor Ba(Fe$_{1-x}$Co$_x$)$_2$As$_2$ across the Superconducting Dome

Lan Luan, Thomas M. Lippman, Clifford W. Hicks,[*] Julie A. Bert, Ophir M. Auslaender,[†] Jiun-Haw Chu, James G. Analytis, Ian R. Fisher, and Kathryn A. Moler[‡]

Stanford Institute for Materials and Energy Science, SLAC National Accelerator Laboratory, 2575 Sand Hill Road, Menlo Park, California 94025, USA, and Geballe Laboratory for Advanced Materials, Stanford University, Stanford, California 94305, USA

We measure the penetration depth $\lambda_{ab}(T)$ in Ba(Fe$_{1-x}$Co$_x$)$_2$As$_2$ using local techniques that do not average over the sample. The superfluid density $\rho_s(T) \equiv 1/\lambda_{ab}(T)^2$ has three main features. First, $\rho_s(T = 0)$ falls sharply on the underdoped side of the dome. Second, $\lambda_{ab}(T)$ is flat at low T at optimal doping, indicating fully gapped superconductivity, but varies more strongly in underdoped and overdoped samples, consistent with either a power law or a small second gap. Third, $\rho_s(T)$ varies steeply near T_c for optimal and underdoping. These observations are consistent with an interplay between magnetic and superconducting phases.

The magnetic penetration depth λ is one of the most important length scales in superconductors [1]. Its temperature evolution is a sensitive probe of the superconducting gap structure [2,3] and its value is related to the density of electrons in the superconducting state, the superfluid density $\rho_s(T) \equiv 1/\lambda(T)^2$. Comparing $\rho_s(T)$ from samples across the phase diagram of a family of iron pnictide superconductors can shed light on the pairing mechanism [4] as well as on the relation between superconductivity and adjacent phases [5]. The family of Ba(Fe$_{1-x}$Co$_x$)$_2$As$_2$ is a good candidate for such studies because single crystals can be grown cleanly with relatively sharp superconducting transitions [6,7], because the magnetic and structural transitions are well characterized [8–10], and because other careful studies of quasiparticle excitation measurements such as thermal conductivity [11,12] and Raman scattering [13] have been successfully performed across the phase diagram.

λ is difficult to measure accurately. In the pnictides, the proximity of the magnetic phase to superconductivity on the underdoped (UD) side of the superconducting dome prevents measurement of λ by μSR [14]. Bulk measurements by microwave- and rf-based techniques are made difficult by complex sample topography and inhomogeneity, which may explain the significantly different results among nominally similar samples of both $\Delta\lambda \equiv \lambda(T) - \lambda(0)$ [15–19] and λ [20] measurements. Local-probe studies of $\rho_s(T)$ across the doping range are strongly desirable, because such measurements can obtain λ even when the magnetic order is adjacent or coexisting [21], and can reduce the error from topography and inhomogeneity [22].

In this Letter, we report local measurements of $\lambda_{ab}(T)$, the penetration depth for screening currents flowing in the ab plane in a set of Ba(Fe$_{1-x}$Co$_x$)$_2$As$_2$ single crystals grown from self-flux [7]. We measure at Co composition x across the superconducting dome: underdoped (UD)

$x = 0.045$, 0.049, 0.051; optimally doped (OptD) $x = 0.07$; and overdoped (OD) $x = 0.085$, 0.11. (For UD samples, $\lambda_a \neq \lambda_b$, our measurements give $\lambda_{ab} \equiv \sqrt{\lambda_a \lambda_b}$.) Our measurements average over a few microns. The positions we choose to measure show strong, uniform diamagnetic response, and are at least 15 μm away from topographic steps larger than 0.5 μm. We are able to resolve well-formed vortices to rule out granularity on submicron scales except at $x = 4.5\%$. We observe systematic evolution of $\rho_s(T)$ with x. Our observations suggest strong correlation between magnetism and superconductivity.

We use magnetic force microscopy (MFM) to measure $\lambda_{ab}(T)$ and $\Delta\lambda_{ab}(T) \equiv \lambda_{ab}(T) - \lambda_{ab}(0)$ irrespective of adjacent magnetic states from 5 K to the superconducting transition temperature T_c [21]. We also use scanning superconducting quantum interference device susceptometry (SSS) in a ^{3}He cryostat to measure $\Delta\lambda_{ab}(T)$ from 0.4 to 7 K [22]. Both techniques measure the diamagnetic response to a local field source (either the MFM tip or the SQUID field coil) in the Meissner state. This is measured by SSS through the mutual inductance between the field coil and the pickup loop, and by MFM through the derivative of the vertical component of the force between the magnetic tip and the sample $\partial F_z/\partial z$, where z is the tip-sample distance. The diamagnetic response can be approximated as a time-reversed mirror of the source reflected about a plane λ_{ab} below the surface when the field source is much farther than λ_{ab} above the surface [23]. Under this approximation, changes in z and λ are equivalent, allowing model independent measurement of $\Delta\lambda_{ab}(T)$ that does not depend on the sensor geometry. We determine $\Delta\lambda_{ab}(T)$ by both techniques with 7% error, mostly from calibration uncertainty of the scanner [21,22].

We determine $\lambda_{ab}(T)$ from 5 K to T_c by MFM within 15% error by modeling the MFM tip-superconductor interaction, as described in Ref. [21]. The error mostly comes
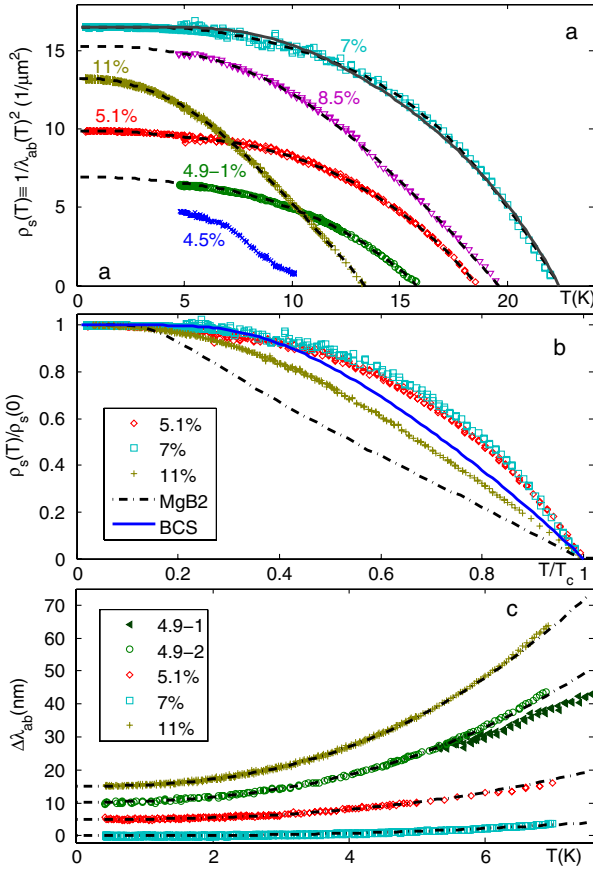
FIG. 1 (color online).   The temperature dependence of $\rho_s(T) \equiv 1/\lambda_{ab}(T)^2$ and $\Delta\lambda_{ab}(T)$ shows three systematic trends. (a) $\rho_s(T)$ vs T. Solid line: a single-gap equation [Eq. (1)] fits only $x = 7\%$. Dashed lines: phenomenological two-gap fits [Eq. (2)] work well at every doping (fit parameters in Table. I). At $x = 8.5\%$, we did not measure $\lambda_{ab}(T)$, so we offset $\Delta\lambda_{ab}(T)$ by the mean of $\lambda_{ab}(0)$ at $x = 7\%$ and $x = 11\%$. (b) $\rho_s(T)/\rho_s(0)$ vs T/T_c. At $x = 5.1\%$ (UD) and $x = 7\%$ (OptD), $\rho_s(T)$ rises more sharply than for MgB$_2$ from Ref. [37], single-band weakly coupled BCS theory, or $x = 11\%$ (OD). (c) $\Delta\lambda_{ab}(T)$ down to 0.4 K measured by SSS at the indicated x. Dashed lines: power-law fits [Eq. (3)] describe the data well up to $0.3T_c$ with the power n fixed at 2.5 (fit parameters in Table. I). The amplitude A increases away from optimal doping, where $\Delta\lambda_{ab}(T)$ is so flat as to be consistent with exponential behavior. $\Delta\lambda_{ab}(T)$ at 5.1%, 4.9%, and 11% are offset vertically by 5, 10, 15 nm, respectively, for clarity. $\Delta\lambda_{ab}(T)$ at $x = 4.9\%$ measured on a different sample by MFM at $T > 5$ K is also plotted.
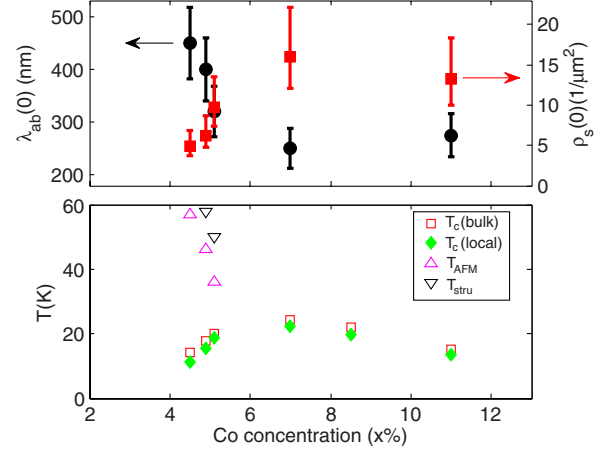

FIG. 2 (color online).   (a) $\lambda_{ab}(0)$ and $\rho_s(0)$ as extrapolated from Fig. 1(a), showing the rapid drop of $\rho_s(0)$ on the underdoped side. For $x = 4.5\%$, $\rho_s(5$ K$)$ is plotted because the extrapolation is unclear. Bars show the errors. (b) Temperatures of structural, magnetic, and superconducting transitions T_{stru}, T_{AFM}, and T_c (bulk), from resistivity measurements of samples from the same growth as studied here. T_c (local) is from linear extrapolation of $\rho_s(T)$ to zero from the MFM data presented here.

from the uncertainty in determining a tip geometry parameter used in the model. We use the same MFM tip at $x = 4.5\%$, 7%, and 11%, reducing the relative error of $\lambda_{ab}(T)$ among these samples. We have verified in Ref. [21] that two different tips give the identical result of λ. A calibration of the technique was performed on YBa$_2$Cu$_3$O$_{6+x}$ single crystals with known λ, which gave good agreement with previously reported value [24].

At most x, we measure at least two samples from the same growth batch, one by MFM and one by SSS. When $\Delta\lambda_{ab}(T)$ measured by both the techniques overlaps in the

common temperature range, we offset $\Delta\lambda_{ab}(T)$ from SSS by $\lambda_{ab}(T = 5$ K$)$ from MFM, and obtain $\rho_s(T) \equiv 1/\lambda_{ab}(T)^2$ over the full temperature range, as shown in Fig. 1. However, $\Delta\lambda_{ab}(T)$ measured by the two techniques do not agree at $x = 4.9\%$, presumably due to sample variations. At $x = 11\%$, we observe different $\Delta\lambda_{ab}(T)$ by SSS at three locations separated by hundreds of microns (shown in Fig. 3), one of which matches the MFM measurement.

We observe a systematic change of $\rho_s(T)$ with Co doping x across the superconducting dome that can be characterized by three trends. First, the zero temperature value $\rho_s(0)$ (Fig. 2) peaks at OptD. It is strongly reduced in the UD regime, falling sharply as the magnetic order onsets. For UD samples, $\rho_s(0)$ falls more quickly than T_c, while on the OD side, $\rho_s(0)$ falls less rapidly than T_c. The values of $\rho_s(0)$ on the OptD and OD samples are in good agreement with μ-sR measurements [14]. Our observation is, however, different from a previous measurement by bulk technique that reported $\rho_s(0)$ increasing with doping across the doping dome [20].

Second, the magnitude of $\Delta\lambda_{ab}(T)$ [Fig. 1(c)] at low T increases away from OptD on both sides of the dome. At $x = 7\%$, $\Delta\lambda_{ab}(T)$ remains flat within 0.5 nm below 3 K, indicating fully gapped superconductivity, consistent with the proposed order parameter $s\pm$ [4]. We use a phenomenological single-gap fit to $\rho_s(T)$ at $x = 7\%$, with the gap function [3]

$$\Delta(T) = \Delta(0)\tanh\left[\frac{\pi T_c}{\Delta(0)}\sqrt{a\left(\frac{T_c}{T} - 1\right)}\right], \quad (1)$$

where a is a free parameter that characterizes the rise of $\rho_s(T)$ below T_c. This full single-gap fit gives $\Delta(0) = 2.0k_BT_c$ and $a = 1.7$, and, as shown in Fig. 1(a), adequately describes the measured temperature dependence for $x = 7\%$.

Because of the steeper $\Delta\lambda_{ab}(T)$ away from OptD, the full single-gap fit does not work at other dopings. The low temperature variation can be described by a power law, but the full temperature dependence is also well described by a two-gap fit with one gap being small. In cases where the SSS and MFM data do not agree or where only one is available, only one of the fits is possible. We use a phenomenological two-gap fit,

$$\rho_s(T) = p\rho_1(T) + (1-p)\rho_2(T), \qquad (2)$$

where ρ_1, ρ_2 are given by Eq. (1) with gaps Δ_1, Δ_2. We fix T_c of the two gaps to be identical and set a for the smaller gap to be 1 to minimize the number of free parameters. Best fit values are shown in Table I. In the power-law description,

$$\Delta\lambda_{ab}(T) = AT^n. \qquad (3)$$

The best fit value of n varied from 2.3 to 2.9, but the error bars for all data sets are consistent with $n = 2.5$. We therefore fixed $n = 2.5$ for simplicity. As shown in Table I, the fitted magnitude of A increases away from OptD.

The third trend we observe is that near T_c, $\rho_s(T)$ of the OptD and UD rises faster with decreasing temperature than weak-coupling BCS theory, MgB_2 or OD [Fig. 1(b)]. This feature is characterized in the full-gap fits: a at $x = 5.1\%$ and 7% are significantly larger than the BCS value $a = 1$, suggesting a steeper rise of $\rho_s(T)$ with cooling than the weakly coupled BCS would give. The same feature is

TABLE I. Fit parameters for curves in Figs. 1 and 3, for the two-gap [Eq. (2)] and power-law [Eq. (3)] models. Power-law fits are based on SSS data and two-gap fits on MFM or combined MFM and SSS data. Where both power-law and two-gap fits are shown, SSS and MFM data on different samples agreed. At $x = 4.9\%$, 5.1% and 7%, $\Delta\lambda_{ab}(T)$ at multiple positions separated by at least 100 μm are identical. For $x = 11\%$, SSS results from three positions are shown. T_c measured on the same sample by MFM or SSS are also provided. See Fig. 1 for an explanation of the two labels for $x = 4.9\%$.

		Full gap				A	
x	T_c (K)	$\frac{\Delta_1}{k_BT_c}$	$\frac{\Delta_2}{k_BT_c}$	a	p	(nm/K$^{2.5}$)	
4.9%-1	15.8	2.2	0.6	1.6	0.90	$\cdots$	$\cdots$
4.9%-2	15.5	$\cdots$	$\cdots$	$\cdots$	$\cdots$	0.26	(3 positions)
5.1%	18.6	2.3	0.7	1.6	0.90	0.09	(4 positions)
7%	22.4	3.3	1.3	1.7	0.70	0.02	(4 positions)
8.5%	19.6	1.9	0.6	1	0.92	$\cdots$	$\cdots$
11%	13.5	1.7	0.6	0.9	0.87	0.38	(position 1)
11%	$\cdots$	$\cdots$	$\cdots$	$\cdots$	$\cdots$	0.27	(position 2)
11%	$\cdots$	$\cdots$	$\cdots$	$\cdots$	$\cdots$	0.18	(position 3)

shown in $\rho_s(T)/\rho_s(0)$ vs T/T_c plots when comparing with other superconductors. The curves at $x = 5.1\%$ (UD) and 7% (OptD) have similar slopes near T_c. Both are steeper than that of MgB_2, a weakly coupled two-gap BCS superconductor; or $x = 11\%$ (OD).

Local probes allow us to measure at multiple positions on multiple samples and to examine real-space inhomogeneity. On all samples we measured with MFM, we obtain identical $\lambda_{ab}(T)$ and $\Delta\lambda_{ab}(T)$ within errors on positions several microns apart. On all samples studied with SSS, we measured three or four positions separated by hundreds of microns. For the $x = 4.9\%$, 5.1%, and 7% samples, the $\Delta\lambda_{ab}(T)$ measurements were identical within errors at each location. We observe spatial variation in $\Delta\lambda_{ab}(T)$ on one $x = 11\%$ sample as shown in Fig. 3, resulting in the variations in fit parameters shown in Table I. In principle, such spatial variations could come from doping inhomogeneity in the sample, or from roughness of the sample surface, or from other variations. In order to quantify doping inhomogeneity in the sample, we performed x-ray microanalysis after the SSS measurement was complete. The 3 μm beam was scanned across a 1.2 mm long line in 20 μm steps. We observe no systematic change in the doping level to within $\pm 2\%$ of the total Co concentration. We do not think the spatial variation comes from sample surface roughness because we checked the topography by susceptometry scans *in situ* and by optical microscopy after the measurement, and because roughness is expected to overestimate $\Delta\lambda$, while the three values are either smaller than or the same as the MFM result.

The systematic trends that we have observed in $\rho_s(T)$ should be considered in light of properties in the superconducting states that are expected to evolve with doping, including the structure of the gap in k space on multiple bands [13,25], magnetic scattering, other forms of scattering [26], and transfer of spectral weight to spin fluctuations and the magnetic phase [27,28]. In particular, the three trends of $\rho_s(T)$ can be accounted for by the interplay between magnetism and superconductivity.

The first trend, $\rho_s(0)$ dropping more rapidly on moving towards UD than towards OD, follows naturally from the fact that the structural and magnetic transitions lead to
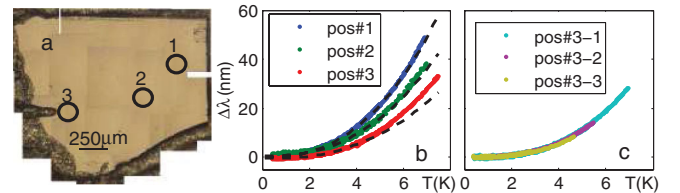

FIG. 3 (color). Inhomogeneity in $\Delta\lambda_{ab}(T)$ observed in an $x = 11\%$ sample. (a) Photograph of the $x = 11\%$ sample measured by SSS. The label of positions corresponds to the position where $\Delta\lambda_{ab}(T)$ was measured. (b),(c) $\Delta\lambda_{ab}(T)$ by SSS at positions 1–3 (b) and three different positions around position 3 each separated by 15 μm (c). Dashed lines in (b) plot power-law fits with parameters given in Table I.

significant Fermi surface reconstruction [25,29], resulting in smaller electron and hole pockets and therefore fewer charge carriers for the superconducting state. In the UD cuprates, the reduction of $\rho_s(0)$ approximately following T_c [30] has been often attributed to phase fluctuations of the superconducting state [31]. We observed an even faster drop of $\rho_s(0)$ than T_c, consistent with the scenario that the coexisting order, e.g., the magnetic order, removes a large number of itinerant carriers that might otherwise enter the superconducting condensate.

The second trend, weakening of fully gapped behavior away from OptD, agrees with heat transport measurements which have also reported an increase in low-energy quasi-particle excitation on either side of OptD [12]. The observation indicates strong pair-breaking scattering or anisotropic superconducting gap structure in the $s\pm$ pairing symmetry [32]. The Fermi surface reconstruction resulting from the magnetic order on the UD side is not expected to lead to nodes, but may result in deep minima in the gap structure [33,34]. The increasing strength of the static order and low-frequency magnetic fluctuations on the UD side [9,10] could enhance pair-breaking magnetic scattering [35], giving rise to a power-law dependence in $\Delta\lambda_{ab}(T)$ [32] that gets sharper with less doping on the UD side. On the OD side, deep gap minima may result from an anisotropic reduction of pairing strength as the doping moves further from the static magnetic order. Although pair breaking may play some role and is one possible explanation for the spatial variation in the 11% sample, two facts suggest that our results are not dominated by pair-breaking processes: the doping dependence we report is consistent with the low-energy excitations measurements on annealed crystals [36], and we observe flat $\Delta\lambda_{ab}(T)$ at OptD.

The third trend, the rapid increase $\rho_s(T)$ of the UD and OptD when cooling through T_c, also agrees with the importance of magnetism. If the pairing is mediated by spin fluctuations [4], forming superconductivity pushes the fluctuation spectrum to higher frequency, which further strengthens pairing, leading to a more rapid rise of $\rho_s(T)$ than the standard BCS expression would give [35]. On the OD side, away from the magnetic order, the absence of low-frequency magnetic fluctuations may contribute to the slow rise of $\rho_s(T)$ when cooling through T_c. The slower rise at $x = 11\%$ than the weak-coupling BCS result may hint that the two gaps have different T_c's.

To conclude, by locally measuring $\lambda_{ab}(T)$ and $\Delta\lambda_{ab}(T)$, we observe systematic doping evolution of both the zero temperature value and the temperature dependence of $\rho_s(T)$ in $Ba(Fe_{1-x}Co_x)_2As_2$ single crystals. Using local scanning techniques, we reduce the error from sample inhomogeneity. The three systematic trends we observe on $\rho_s(T)$ across the superconducting dome are consistent with the role of magnetism as a coexisting and competing order to the superconductivity as well as the pairing glue.

*Present address: School of Physics and Astronomy, University of St. Andrews, North Haugh, St. Andrews, Fife KY16 9SS, United Kingdom.

†Present address: Physics Department, Technion-Israel Institute of Technology, Haifa 32000, Israel.

‡Corresponding author.
kmoler@stanford.edu

[1] M. Tinkham, *Introduction to Superconductivity* (McGraw-Hill, New York, 1975).
[2] W. Hardy *et al.*, Phys. Rev. Lett. **70**, 3999 (1993).
[3] R. Prozorov and R. W. Giannetta, Supercond. Sci. Technol. **19**, R41 (2006).
[4] I. I. Mazin *et al.*, Phys. Rev. Lett. **101**, 057003 (2008).
[5] A. B. Vorontsov, M. G. Vavilov, and A. V. Chubukov, Phys. Rev. B **79**, 060508 (2009).
[6] N. Ni *et al.*, Phys. Rev. B **78**, 214515 (2008).
[7] J.-H. Chu *et al.*, Phys. Rev. B **79**, 014506 (2009).
[8] S. Nandi *et al.*, Phys. Rev. Lett. **104**, 057006 (2010).
[9] C. Lester *et al.*, Phys. Rev. B **79**, 144523 (2009).
[10] D. K. Pratt *et al.*, Phys. Rev. Lett. **103**, 087001 (2009).
[11] M. A. Tanatar *et al.*, Phys. Rev. Lett. **104**, 067002 (2010).
[12] J.-P. Reid *et al.*, Phys. Rev. B **82**, 064501 (2010).
[13] B. Muschler *et al.*, Phys. Rev. B **80**, 180510 (2009).
[14] T. J. Williams *et al.*, Phys. Rev. B **82**, 094512 (2010).
[15] K. Hashimoto *et al.*, Phys. Rev. Lett. **102**, 207001 (2009).
[16] K. Hashimoto *et al.*, Phys. Rev. B **81**, 220501 (2010).
[17] L. Malone *et al.*, Phys. Rev. B **79**, 140501 (2009).
[18] C. Martin *et al.*, Phys. Rev. B **80**, 020501 (2009).
[19] R. T. Gordon *et al.*, Phys. Rev. B **79**, 100506 (2009).
[20] R. T. Gordon *et al.*, Phys. Rev. B **82**, 054507 (2010).
[21] L. Luan *et al.*, Phys. Rev. B **81**, 100501 (2010).
[22] C. W. Hicks *et al.*, Phys. Rev. Lett. **103**, 127003 (2009).
[23] V. G. Kogan, Phys. Rev. B **68**, 104511 (2003).
[24] L. Luan *et al.* (unpublished).
[25] C. Liu *et al.*, Nature Phys. **6**, 419 (2010).
[26] R. T. Gordon *et al.*, Phys. Rev. B **81**, 180501 (2010).
[27] D. S. Inosov *et al.*, Nature Phys. **6**, 178 (2010).
[28] R. M. Fernandes and J. Schmalian, Phys. Rev. B **82**, 014520 (2010).
[29] J. G. Analytis *et al.*, Phys. Rev. B **80**, 064507 (2009).
[30] Y. J. Uemura *et al.*, Phys. Rev. Lett. **62**, 2317 (1989).
[31] V. J. Emery and S. A. Kivelson, Nature (London) **374**, 434 (1995).
[32] A. B. Vorontsov, M. G. Vavilov, and A. V. Chubukov, Phys. Rev. B **79**, 140507 (2009).
[33] D. Parker, M. G. Vavilov, A. V. Chubukov, and I. I. Mazin, Phys. Rev. B **80**, 100508 (2009).
[34] P. Ghaemi and A. Vishwanath, arXiv:1002.4638.
[35] P. Monthoux and D. J. Scalapino, Phys. Rev. B **50**, 10 339 (1994).
[36] K. Gofryk *et al.*, arXiv:1009.1091v2 [Phys. Rev. B (to be published)].
[37] J. D. Fletcher *et al.*, Phys. Rev. Lett. **95**, 097005 (2005).